Research article

polymers advanced technologies

Received: 27 January 2016, Revised: 16 March 2016, Accepted: 17 March 2016, Published online in Wiley Online Library: 7 April 2016

(wileyonlinelibrary.com) DOI: 10.1002/pat.3809

Hydrogen bonding interaction and crystallization behavior of poly (butylene succinate-co-butylene adipate)/thiodiphenol complexes

Pengfei Si[a,b] and Faliang Luo[a,b]*

The poly (butylene succinate-*co*-butylene adipate) (PBSA)/thiodiphenol (TDP) complexes were prepared by melt blending. Intermolecular hydrogen bonding between carbonyl group of PBSA and hydroxyl group of TDP formed as verified by a combination FTIR and peak fitting technique. As a result, the crystallization temperature, melting temperature, crystallinity and crystallization rate of PBSA decreased with addition of TDP, implying impeded crystallization and reduced lamellar thickness. On the basis of Lauritzen–Hoffman analysis, the fold surface energy (σ_e) and work of chain folding (q) were increased by TDP incorporation. POM observation exhibited concentric ring-banded spherulites for samples with 10 and 20 wt% TDP. A peculiar ring-banded pattern with discrepant band spacing was obtained for the first time by addition of 30 wt% TDP, whose formation mechanism remains to be discussed. Copyright © 2016 John Wiley & Sons, Ltd.

Keywords: hydrogen bonding; poly (butylene succinate-*co*-butylene adipate); crystallization; ring-banded morphology

INTRODUCTION

Biodegradable poly (butylene succinate-*co*-butylene adipate) (PBSA) copolymers have been widely studied for both academic and engineering interests.[1–4] The crystallization behavior, lamellae organization and properties of PBSA can be modulated by altering the succinate to adiptae unite ratios.[5–7] However, it still suffers from some limitations in certain applications.

Blending is a favorable approach to obtain materials with elevated properties and cost performances because of simple process and easy adoption in mass production.[8,9] Especially, potential specific intermolecular interactions are intentionally designed on basis of chemical structure to enhance miscibility between components in blending systems, such as ion-dipole, π–π and hydrogen bonding interactions.[10] Intermolecular hydrogen bonding is prone to form between nucleophilic ester groups and groups that donate protons, and therefore frequently engaged in recent research concerning polyester modifications. For example, poly (vinyl phenol), phenolic, phenoxy and tannic acid had been reported miscible with poly (butylene succinate) (PBS),[11,12] PBSA[13,14] and poly (ε-caprolactone) (PCL),[15] and significantly influenced crystallization behavior and serving properties of these polyesters as a result of intermolecular hydrogen bonding interaction. In addition, some low molecular weight *n*-alkyl carboxylic acids had also been utilized to improve the thermal and mechanical properties of polyesters by forming peculiar structures. One typical case is that amphiphilic octadecanoic acid obviously improved the thermal degradation temperature of poly (propylene carbonate) because of the formation of thermotropic liquid crystalline complex, which extended its potential applications.[16]

Some low molecular weight dihydric phenols can be used as antioxidants and thermal stabilizer in polymer processing,[17] which also have been reported to have the capability to form hydrogen bonding interaction with polyesters owing to electrophilic hydroxyl groups in molecular structure. Moreover, the mobility of dihydric phenols and the dynamic character of hydrogen bonding motivated researchers to investigate the impacts of incorporation of dihydric phenols on properties of polyesters,[18] For instance, a series of dihydric phenols including TDP, bisphenol A (BPA), 4,4′-dihydroxydiphenyl mechane (DHDPM) and 4,4′-dihydroxydiphenyl ether (DHDPE) had been incorporated into PBS, PCL, poly (3-hydroxybutyrate-*co*-3-hydroxyvalerate) (PHBV), Poly (3-hydroxybutyrate), poly (L-lactic acid), etc.[18–22] The crystallization behavior and morphologies of the polyesters were modified as a result of hydrogen bonding

* *Correspondence to: Professor Faliang Luo, Key Laboratory of Energy Resource and Chemical Engineering, Ningxia University, Yinchuan 750021, China. E-mail: flluo@iccas.ac.cn*

a *P. Si, F. Luo*
Key Laboratory of Energy Resource and Chemical Engineering, Ningxia University, Yinchuan 750021, China

b *P. Si, F. Luo*
School of Chemistry and Chemical Engineering, Ningxia University, Yinchuan 750021, China

Abbreviations used: *PBSA, poly (butylene succinate-co-butylene adipate); PBS, poly (butylene succinate); PCL, poly (ε-caprolactone); PHBV, poly (3-hydroxybutyrate-co-3-hydroxyvalerate); TDP, thiodiphenol; FTIR, Fourier transform infrared spectroscopy; DSC, differential scanning calorimetry; WAXD, wide angle X-ray diffraction; POM, polarized optical microscopy; T_m, melting peak temperature; T_c, crystallization peak temperature; ΔH_m, melting enthalpy; ΔH_c, crystallization enthalpy; PWHM, peak width at half maximum; n, Avrami exponent; k, crystallization rate constant; $t_{1/2}$, half crystallization time; T_m^o, equilibrate melting temperature; K_g, nucleation constant; σ, side surface; σ_e, fold surface energy; q, work of chain folding*

network, and some novel properties were obtained. For the dihydric phenols in these complexes, polarity of the group linking two hydroxyphenyls and flexibility of the molecular chain significantly affect the tendency and strength of hydrogen bonding formation.[21] It is obvious that TDP molecule is more flexible than DHDPE as shown in Scheme 1. Because the sulfur atom between two *p*-hydroxyl phenols in TDP has larger size than that of oxygen atom in DHDPE, the bond length of C—S—C is longer than that of C—O—C. While DHDPE possess better flexibility than DHDPM and BPA because of steric effect caused by hydrogen atoms or methyl groups around carbon atom between two *p*-hydroxyl phenols in DHDPM and BPA molecules. Thus, TDP is supposed to an ideal dihydric phenol to form hydrogen bonding with polyesters. In the present work, we systematically investigated the hydrogen bonding interaction in PBSA/TDP complexes and its influence on crystallization behavior, crystal structure and morphology of PBSA, attempting to develop an effective approach to regulate crystallization of polyesters.

EXPERIMENTAL

Materials

Poly(butylene succinate-co-butylene adipate) (PBSA) with ca. 5 mol% adipate unite was purchased from Anqing He Xing Chemical Co. Ltd. (China) in the form of small granules. The weight-average molecular weight (M_w) and number-average molecular weight (M_n) determined by GPC method using chloroform as solvent were 9.5×10^4 and 4.8×10^4, respectively. PBSA granules were dried prior to use in vacuum at 60°C for 24 hr to remove any residual moisture. TDP with a melting point of 154°C was purchased from Meryer (Shanghai) Chemical Technology Co. Ltd. and used as received. The molecular structures of PBSA and TDP are presented in Scheme 1.

Sample preparation

PBSA and PBSA/TDP complexes were prepared via melt blending method using a minitype twin screw extruder (Rui Ming plastic machinery manufacturing Co., Ltd., China). PBSA and TDP in predesigned weight ratios were fully blended in the extruder at 160°C, which is above the melting temperature of both PBSA and TDP. The resulting products were cooled in air and collected for characterization.

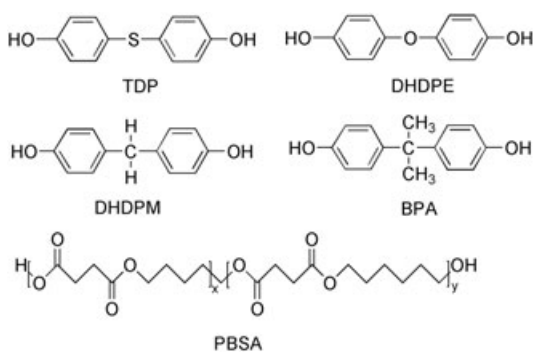

Scheme 1. Chemical structures of PBSA and some dihydric phenols.

Measurements

FTIR

Thin films with suitable thickness for IR measurement were prepared by dropping sample solution in chloroform directly onto the surfaces of KBr wafers. The solvent was allowed evaporate in air. Residual solvent in the resulting thin films was removed by drying in vacuum at 60°C for 24 hr. IR measurements were carried out on a Bruker Tensor27 spectrometer (Germany) in absorbance mode at a resolution of 4 cm^{-1} with an accumulation of 32 scans.

DSC analysis

DSC analysis was performed on a TA DSC-Q20 instrument (USA) with a universal analysis 2000 under nitrogen purge. For non-isothermal melt crystallization and subsequent melting behavior, scanning rate for all samples was 10°C/min. Samples of ca. 5 mg were encapsulated in aluminum pans and heated to 160°C, held for 5 min to eliminate any thermal history, followed by cooling down to 0°C and finally reheated to 160°C. For isothermal melt crystallization behavior, the molten state samples were cooled rapidly to preselected temperatures and maintained long enough until heat flow did not vary with time, The subsequent heating curves with a scanning rate of 10°C/min were also recorded.

Wide angle X-ray diffraction (WAXD) measurement

Molten state samples were pressed into sheets for WAXD measurement. WAXD was carried out on a Rigaku D/max2000PC diffractometer (Japan) at a scanning rate of 2°/min in the range of 5–40°. Monochromatized Cu Kα radiation (λ = 1.542 Å) was used as incident X-ray beam. Tube voltage and current were set as 40 kV and 30 mA, respectively.

Polarized optical microscope (POM) observation

A Leica DM 2500P (Germany) POM equipped with a hot stage was utilized for the observation of morphological change. The samples were melted at 160°C and pressed into thin films between two glass slides, followed by free cooling to ambient temperature. The thin films were transferred to a hot stage mounted on POM, heated to 160°C and held for 3 min, then cooled to 20°C at a cooling rate of 2°C/min. Micrographs were captured during cooling process.

RESULTS AND DISCUSSION

Intermolecular interactions between PBSA and TDP

It is known that hydroxyl groups afford a proton and are expected to form hydrogen bond with nucleophilic carbonyl groups, which can be verified by infrared spectroscopy. The FTIR spectra of neat PBSA, TDP and PBSA/TDP complexes are presented in Fig. 1. On basis of Beer–Lambert law, the absorbance intensities of PBSA and complexes are normalized. As can be seen from Fig. 1(a), strong absorption bands around 3410 cm^{-1} caused by hydroxyl group stretching vibration appear on FTIR spectrum of TDP. While vibration of terminal hydroxyl groups in PBSA give rise to a very weak band at 3438 cm^{-1} because of high molecular weight of PBSA. Therefore, the increase in intensity for complexes shown in Fig. 1(a) is obviously

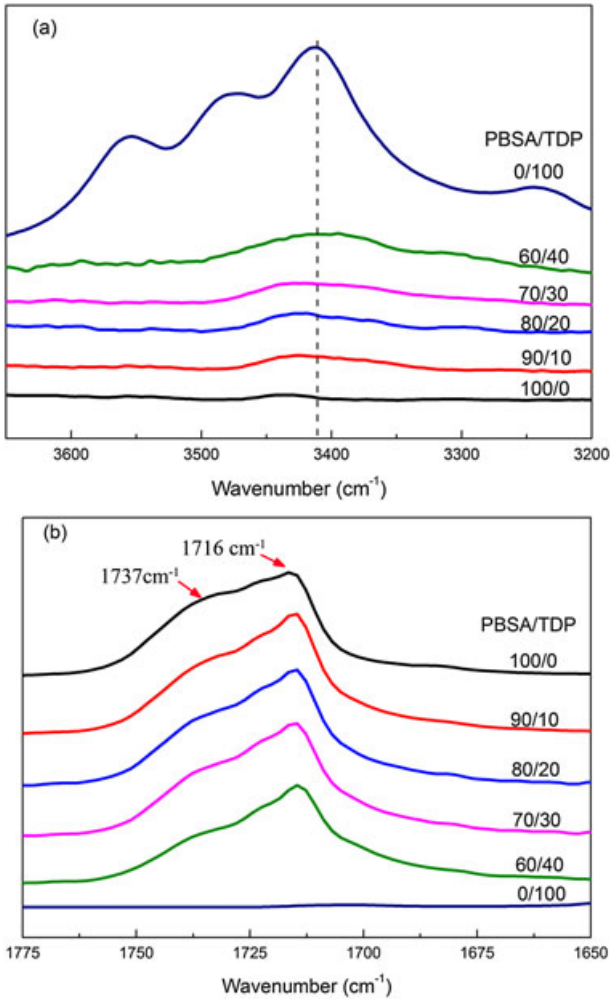

Figure 1. FTIR spectra of PBSA and the complexes in (a) hydroxyl group and (b) carbonyl group vibration region.

owing to increasing TDP content. However, when comparing the spectra for TDP with that for complexes, we found non-negligible differences in band location. The hydroxyl vibration absorption bands for TDP shift to higher wavenumber after incorporated into PBSA. The band shifting indicates that hydroxyl groups of TDP formed intermolecular hydrogen bonds with carbonyl groups of PBSA.

Besides, notable changes in carbonyl vibration absorption bands have also been observed as shown in Fig. 1(b). The strong carbonyl absorption band for PBSA actually contains two overlapping peaks. It is quite common that crystalline polyesters possess at least two absorption peaks in carbonyl stretching region, usually the one at higher wavenumber resulting from carbonyl stretching in amorphous part and the other one at lower wavenumber originating from crystalline component. For example, absorption peaks at 1740 cm^{-1} and 1723 cm^{-1} originating from carbonyl absorption in amorphous and crystalline component, respectively, had been distinguished for PHBV.[18] A more similar example to PBSA is the case of PBS, whose amorphous and crystalline carbonyl absorption being identified at 1738 cm^{-1} and 1722 cm^{-1}, respectively.[19] Therefore, for PBSA with only 5 mol% of BA unit in this work, the shoulder peak at higher wavenumber (1737 cm^{-1}) and the most obvious peak at lower wavernumber (1716 cm^{-1}) are assigned to stretching vibration of carbonyl in amorphous and crystalline component, respectively. The intensity of the peak at 1737 cm^{-1} decreases relative to that at 1716 cm^{-1}. This can be attributed to fractional changes of crystalline, amorphous and hydrogen bonded carbonyl groups, which can be legibly discerned using a peak fitting software *Peakfit*. This software detects hidden peaks by second derivative minima. The program adjusts the peak location, line shape, peak width and height based on least-squares parameter-adjustment criterion using the Gauss amplitude function to obtain the best fit.

The experimental and fitted spectra of PBSA/TDP 60/40 are presented in Fig. 2 as a typical example. It can be seen that the second derivative curve in Fig. 2(a) exhibits six local minima, which theoretically indicates six potential hidden peaks exist at corresponding wavenumbers on experimental observed spectrum. Whereas the intensities at 1768, 1697 and 1661 cm^{-1} being within or very close to baseline, these peaks are considered as noise and thus discarded by setting appropriate amplitude threshold value. As a result, the hidden peak indicated by minima at 1697 cm^{-1} on second derivative curve is located at 1692 cm^{-1} on basis of the algorithm adopted by the program. The local peak resolved at 1737 and 1716 cm^{-1} is in well accordance with that determined by second derivative minima. Good agreement between experimental and fitted spectra shown in Fig. 2(b) also indicates excellent reliability of the peak

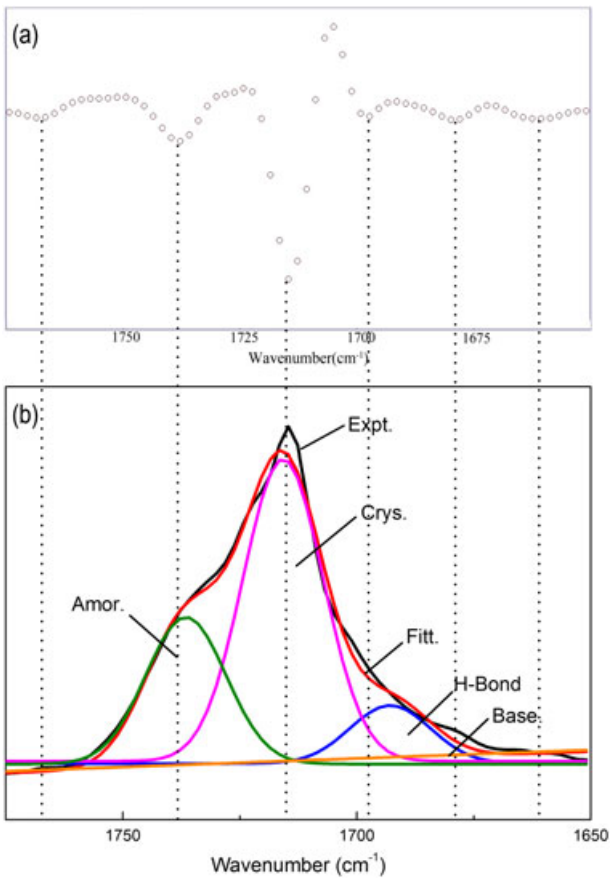

Figure 2. (a) Second derivative of PBSA/TDP 60/40 spectrum; (b) experimental and fitted IR spectra of PBSA/TDP 60/40. Expt: experimental spectrum; Fitt: fitted spectrum; Cry: crystalline component; Amor: amorphous component; H-Bond: hydrogen bonded component; Base.: baseline.

fitting program. As can be seen, the $\nu_{C=O}$ stretching mode of 1737 cm^{-1} ascribing to amorphous carbonyl red shifts to 1692 cm^{-1} after forming hydrogen bonding with hydroxyl group of TDP. The relative area (A_i) of corresponding fitted peaks, which had also been obtained from the fitting program, is used for quantitatively analyzing the variations of fractions of three components. That is, $f_i = A_i / \sum A$. The calculated fractions of three components are listed in Table 1. It can be seen that fraction of crystalline component remains almost unchanged with increasing TDP content, while fraction of hydrogen bonded carbonyl groups increases at the expense of non-hydrogen bonded amorphous carbonyl groups.

DSC analysis

Non-isothermal crystallization and subsequent melting DSC curves of PBSA and PBSA/TDP complexes are shown in Fig. 3. The melting and crystallization temperatures are taken as the temperatures corresponding to peak maximums, and denoted as T_{mp} and T_{cp}, respectively. As can be seen from Fig. 3(a), the T_{cp} of PBSA is around 58.7°C with a crystalline enthalpy (ΔH_c) of −61.5 J/g. While those for complexes successively decrease with increasing TDP content. The T_{cp} shifts to 31.8°C with a ΔH_c of −31.9 J/g when incorporated 30 wt% of TDP into PBSA, which is also listed in Table 2. This means that crystallization of PBSA was retarded. TDP molecules were linked to PBSA chains via H-bonding and may act as side groups or crossing linking agents. As a result, the mobility of PBSA chains decreased, leading to lower nucleation rates and hindered crystal growth. In addition, the crystallization peak with at half maximum (*PWHM*), proposed by many researchers to evaluate the crystal size distribution,[23] increases with TDP as listed in Table 2, implying that spherulitic size of PBSA become less uniform in the presence of TDP. The effects of TDP introduction on crystallinity of PBSA were estimated using the following equation:

$$X_C = \frac{\Delta H_c}{110.5 \times (1 - W)} \quad (1)$$

where X_c is the crytallinity of PBSA in samples, W is the weight fraction of TDP and the constant 110.5 J/g is the heat of fusion for 100% crystalline PBSA. The calculated results are listed in Table 2. As can be seen, X_c for PBSA/TDP complexes generally decreases with TDP addition, which means that crystallization of PBSA was retarded.

Figure 3(b) shows the subsequent melting DSC curves of PBSA and the complexes. A sharp melting endothermic peak around 154°C appears on heating curve of TDP. However, no endothermic peaks were present at the corresponding location on heating curves of the complexes, meaning that TDP was in amorphous state in PBSA–TDP complexes in investigated extent. The T_{mp} of PBSA decreased distinctly with increasing TDP content, implying that the lamellar thickness was reduced.

The glass transition temperatures (T_g) for PBSA and PBSA/TDP complexes are listed in Table 2. As can be seen, the T_g increases with TDP addition, meaning that mobility of PBSA chains was reduced because of hydrogen bonding formation.

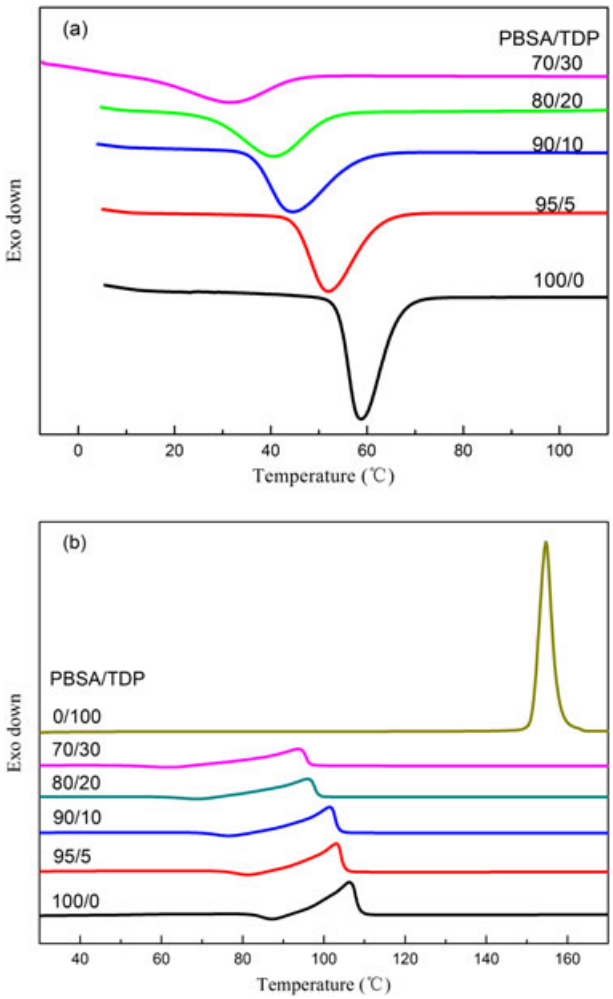

Figure 3. (a) DSC curves of PBSA and the complexes crystallized from the melt; (b) DSC curves of subsequent melting process for PBSA and the complexes.

Table 1. Calculated fractions of crystalline, amorphous and hydrogen bonded carbonyl groups in PBSA and the complexes

Samples	$F_{(A,C=O)}$(%)[1]	$F_{(C,C=O)}$(%)[2]	$F_{(H,C=O)}$(%)[3]
PBSA/TDP 100/0	40.3	59.7	—
PBSA/TDP 90/10	33.4	58.6	8.0
PBSA/TDP 80/20	33.3	58.5	8.2
PBSA/TDP 70/30	32.5	58.2	9.3
PBSA/TDP 60/40	28.9	59.6	11.5

[1]Fraction of amorphous carbonyl groups.
[2]Fraction of crystalline carbonyl groups.
[3]Fraction of hydrogen bonded carbonyl groups.

Isothermal crystallization and subsequent melting process

PBSA and the complexes containing 2, 4 and 6 wt% of TDP are selected for the study of isothermal crystallization behavior, on account that samples with higher TDP contents crystallize so slow that it would be difficult for comparison under same crystallization temperatures. DSC exothermic curves were obtained by quenching the melt to preselected temperature range of 76–80°C and maintaining long enough to allow complete crystallization. The symmetrical profile of the crystallization curves presented in Fig. 4(a) suggests that the

Table 2. DSC data for nonisothermal crystallization, melting and glass transition behaviors

Samples	T_{cp}(°C)	ΔH_c(J/g)	X_c(%)	*PWHM*(°C)	T_{mp}(°C)	ΔH_m(J/g)	T_g(°C)
PBSA/TDP 100/0	58.7	−61.5	55.8	7.5	106.3	60.2	−35.5
PBSA/TDP 95/5	52.0	−55.8	53.3	10.4	102.9	58.0	−34.3
PBSA/TDP 90/10	44.5	−53.4	53.8	12.8	101.5	54.2	−30.2
PBSA/TDP 80/20	40.6	−41.9	47.4	14.4	96.0	51.8	−28.8
PBSA/TDP 70/30	31.8	−31.9	41.3	17.9	93.7	52.0	−28.5

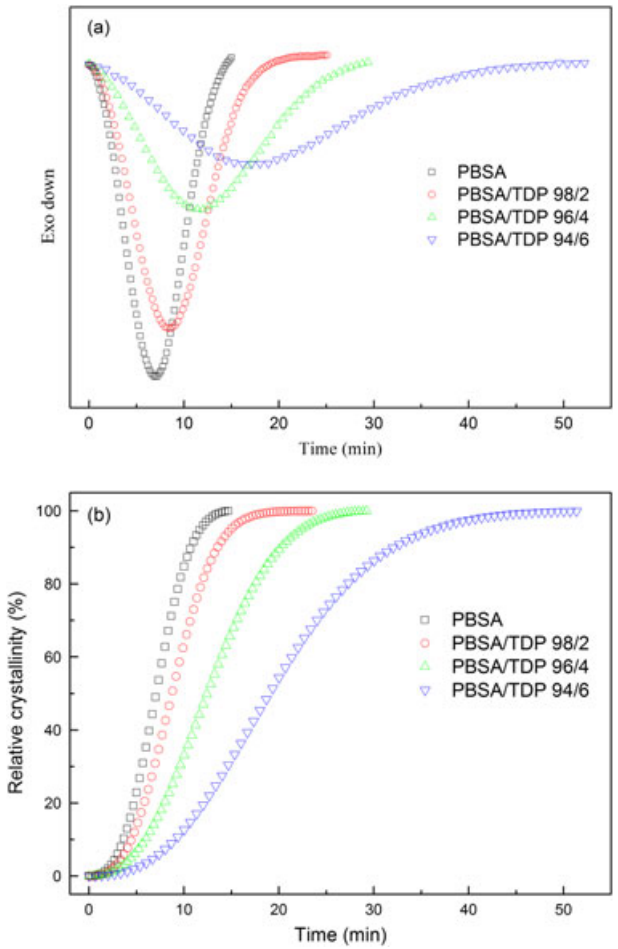

Figure 4. (a) DSC heat flow and (b) relative crystallinity as a function of time for PBSA and the complexes isothermally crystallized at 80°C.

isothermal crystallization process of PBSA did not present any secondary crystallization.

The development of relative crystallinity with time shown in Fig. 4(b) can be analyzed with Avrami equation[24]:

$$1\text{-}X_t = \exp(-kt^n) \quad (2)$$

where X_t is the relative crystallinity at time t, k is crystallization rate constant and n is the Avrami exponent dependent on crystallization mechanism and spherulite growth dimensions. Using the double logarithmic form of eqn (2), one can obtain n and k values from slopes and intercepts of plots of $\ln[-\ln(1-X_t)]$ versus $\ln t$, respectively. Figure 5 shows the Avrami plots of samples crystallized at designated temperatures. Good alignments on straight lines form for PBSA in full relative crystallinity range at all investigated crystallization temperatures. However, deviations from Avrami plots occur in early stage of isothermal crystallization after incorporation of TDP in PBSA matrixes. The deviation in primary crystallization stage is generally considered to originate from crystallization induction effect.[7,25]

The linear portions in relative crystallinity range of 2–100% were used for data fitting to acquire crystallization kinetic parameters. The n values of PBSA and the complexes are between 2.4 and 2.8 as listed in Table 3. Theoretically, the value of n should be integers depending on nature of spherulite growth and nucleation mechanism. While under experimental conditions, n values are usually non-integer between 2 and 5.4 dependent on different crystallization mechanism and testing techniques.[26] The non-integer n values between 2.4 and 2.8 in this work suggest that spherulites assumed a two-dimensional to three-dimensional growth with a combination of homogeneous and heterogeneous nucleation in PBSA/TDP complexes.

Overall crystallization rate can be evaluated by the parameter $t_{1/2}$, the time needed to complete half of crystallization. Figure 6 shows the effects of TDP introduction on $t_{1/2}$ of samples crystallized at indicated temperatures. It is clear that $t_{1/2}$ increases with TDP content and crystallization temperatures, suggesting that crystallization rate of PBSA was reduced.

The subsequent melting curves of PBSA/TDP 94/6 after isothermally crystallized at designated temperatures are illustrated in Fig. 7 as a typical example. Double melting peaks are observed for all samples. This is a common phenomenon for many polyesters, which can be interpreted as melt-recrystallization mechanism.[11,27] The endothermic peak located at lower temperature (T_{m1}) is attributed to the melting of crystals formed during isothermal crystallization, while the higher one (T_{m2}) is ascribed to melting of recrystallized crystals during heating process. As can be seen in Fig. 7, T_{m1} successively shifts to higher temperatures with increasing isothermal crystallization temperatures, while T_{m2} remains almost unchanged. Obviously, the thickness of lamellae formed during isothermal crystallization increased with increasing crystallization temperature. Variations of T_{m1} and T_{m2} with the incorporation of TDP are also listed in Table 3.

Determination of equilibrium melting temperature (T_m^o) is necessary here for the convenience of further crystallization kinetics analysis. T_m^o can be deduced on the basis of linear Hoffman–Weeks extrapolative method.[28] Apparent melting temperatures of crystals formed during isothermal crystallization process (T_{m1}) were plotted against isothermal crystallization temperatures, and extrapolated to the line $T_m = T_c$ as shown in Fig. 8. The calculated values of T_m^o for PBSA and the complexes are listed in Table 3. T_m^o of PBSA was estimated to be 123.7°C,

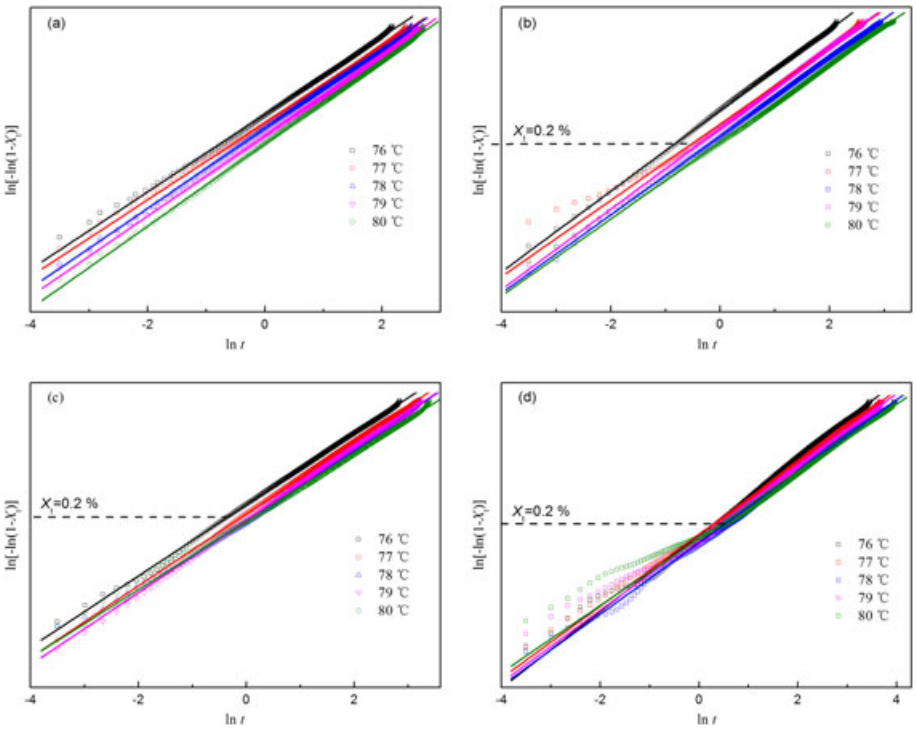

Figure 5. Avrami plots for PBSA and the complexes isothermally crystallized at indicated temperatures; (a) PBSA, (b) PBSA/TDP 98/2, (c) PBSA/TDP 96/4 and (d) PBSA/TDP 94/6.

Table 3. Isothermal crystallization kinetic parameters based on Avrami analysis

Samples	T_c (°C)	T_{m1} (°C)	T_{m2} (°C)	n	$t_{1/2}$ (min)	T_m^o (°C)
PBSA/TDP 100/0	76	93.3	106.1	2.7	3.9	123.7
	77	94.1	106.1	2.7	4.8	
	78	94.7	106.3	2.7	5.1	
	79	95.3	106.3	2.8	6.2	
	80	95.9	106.3	2.8	7.1	
PBSA/TDP 98/2	76	93.0	106.0	2.7	4	125.7
	77	93.5	105.4	2.8	5.2	
	78	94.1	105.5	2.8	5.7	
	79	94.9	105.8	2.7	7.3	
	80	95.6	106.0	2.7	8.8	
PBSA/TDP 96/4	76	92.1	103.9	2.5	6.8	126.6
	77	92.7	103.9	2.5	8.5	
	78	93.3	103.9	2.5	10.1	
	79	94.2	104.4	2.5	10.4	
	80	94.7	104.3	2.5	12.5	
PBSA/TDP 94/6	76	91.6	103.2	2.5	11.9	126.9
	77	92.2	103.3	2.4	13.7	
	78	92.9	103.4	2.5	15.5	
	79	93.5	103.2	2.5	17.9	
	80	94.4	103.2	2.4	19.6	

and that shifts to higher values with increasing TDP mass fraction.

Analysis based on Lauritzen–Hoffman equation

The $t_{1/2}$ as a strong function of T_c can be considered inversely proportional to spherulite growth rate (G) using a theoretical approach, that is, $G = 1/t_{1/2}$. In consequence, the relationship between $t_{1/2}$ and T_c can be written as follows according to Hoffman–Lauritzen equation[29]:

$$\frac{1}{t_{1/2}} = \left(\frac{1}{t_{1/2}}\right)_0 exp\left[-\frac{U}{R(T_C - T_\infty)}\right] exp\left[-\frac{K_g}{T_C \Delta T f}\right]. \quad (3)$$

The first exponential in this equation dominates crystallization rate variations at high supercooling degree. The chain mobility controls the overall crystallization rate, which decreases when temperature approaching T_g of the polymer.[30] U is the activation energy for transferring crystallizable segments to the

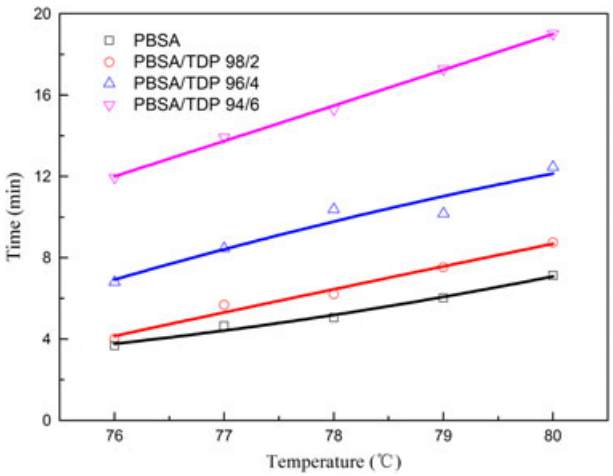

Figure 6. $t_{1/2}$ as a function of isothermal crystallization temperatures and TDP content.

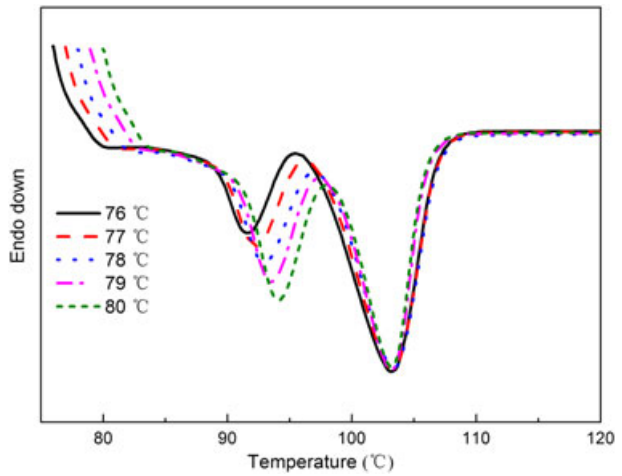

Figure 7. DSC melting curves for PBSA/TDP 94/6 after isothermally crystallized at designated temperatures.

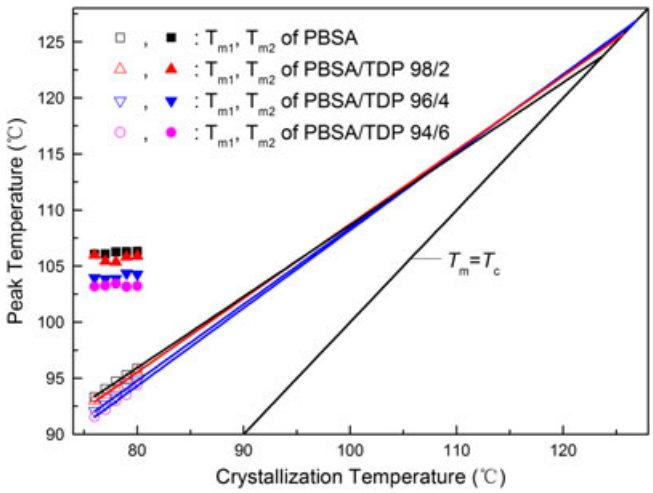

Figure 8. Low and high melting peak temperatures versus crystallization temperatures.

site of crystallization and equals 6300 J/mol as reported[7]; R is the gas constant; T_∞ is the temperature below which the polymer chains lose mobility, usually taken as 30 K below T_g. The second exponential contains thermodynamic terms which account for the driving force of crystallization.[30] K_g is the nucleation constant; ΔT is the supercooling, $\Delta T = T_m^o - T_c$; f is the factor $2T_c/(T_m^o + T_c)$ that accounts for the change of heat of fusion as temperature decreases below T_m^o.

Logarithmic transformation of eqn (3) is usually adopted for the calculation of K_g. The plot of ln $G + U/R(T_c - T_\infty)$ versus $1/T_c\Delta Tf$ should produce a line with $-K_g$ being the slop and the intercept as ln G_0, which is presented in Fig. 9. $T_g = 237.8$ K and T_m^o values listed in Table 3 were utilized for calculation of K_g. The results are listed in Table 4.

The nucleation constant K_g is defined as:

$$K_g = \frac{rb_0\sigma\sigma_e T_m^O}{k\Delta H_f^O} \tag{4}$$

where $b_0 = 0.404$ nm, is the layer thickness; σ and σ_e are side surface and fold surface energy of growing crystal; k is Boltzmann constant; ΔH_f^o is heat of fusion per unit volume,

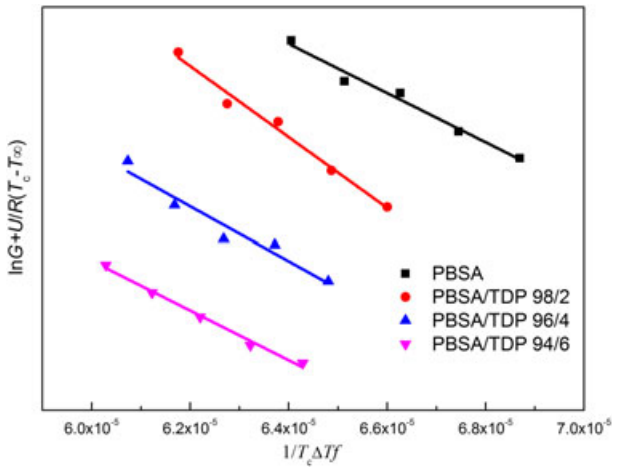

Figure 9. Plots of ln $G + U/R(T_c - T_\infty)$ versus $1/T_c\Delta Tf$ for PBSA and the complexes.

Table 4. K_g, σ_e and q derived from Lauritzen–Hoffman equation

Sample	$K_g \times 10^{-5}$(K^2)	$\sigma_e \times 10^2$ (J/m^2)	$q \times 10^{-3}$ (J/mol)
PBSA/TDP 100/0	1.25	2.34	5.98
PBSA/TDP 98/2	1.81	3.37	8.61
PBSA/TDP 96/4	1.38	2.56	6.54
PBSA/TDP 94/6	1.26	2.34	5.98

reported value 1.47×10^8 J/m^3 was used in this work[7]; r is dependent on crystallization regime and assumes the value of 4 for regime I and III, and 2 for regime II. The T_cs investigated in this work are within regime III according to reported literatures.[7] Thus, $r = 4$ is taken for further analysis of σ_e and work of chain folding on basis of the following empirical formula:

$$\sigma = \alpha(a_0 b_0)^{1/2}\Delta H_f^O \tag{5}$$

$$q = 2a_0 b_0 \sigma_e \tag{6}$$

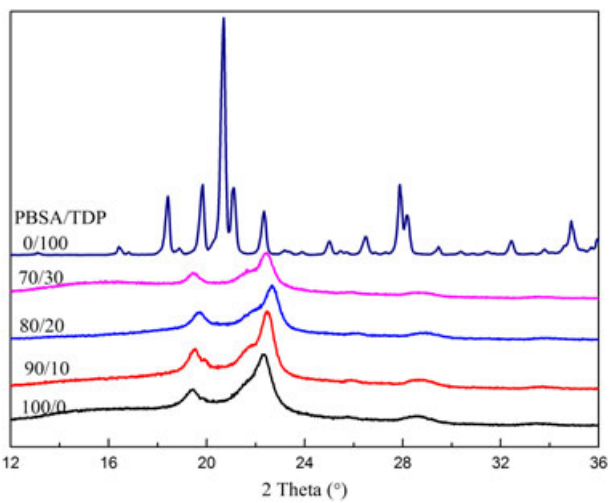

Figure 10. WAXD patterns of neat PBSA, TDP and the complexes.

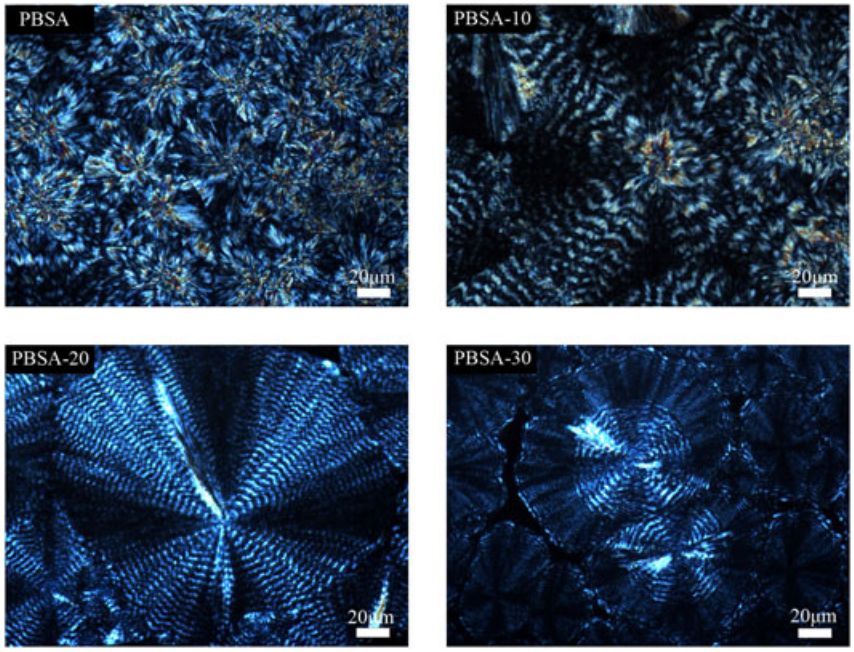

Figure 11. POM images of samples cooling from the melt to 20°C.

where α is an empirical constant, usually taken as 0.1 and 0.25 for polyolefins and polyesters, respectively. Thus, $\alpha = 0.25$ was used here for PBSA. a_0 is the width of a molecular chain, $a_0 = 0.525$ nm. Based on these parameters, σ for PBSA was estimated as 1.69×10^{-2} J/m^2.[7] Accordingly, σ_e and q values for PBSA and the complexes were calculated and listed in Table 4. The increased q values by TDP addition may account for retarded crystallization of PBSA.

WAXD analysis

The WAXD patterns of PBSA, TDP and their complexes are illustrated in Fig. 10. The WAXD pattern of pristine PBSA exhibits five peaks at 19.4, 21.6, 22.4, 25.9 and 28.8 ° 2θ angles, which can be assigned to (11$\bar{1}$) and (202), (012), (110), 12$\bar{1}$ and (111) crystallographic planes, respectively.[31] Diffraction peaks of the complexes are almost identical in 2θ angle with that of neat PBSA, indicating that the introduction of TDP did not modify the crystal structure of PBSA. In addition, note that the characteristic diffraction peaks of neat TDP are absent on WAXD patterns of the complexes, confirming that TDP was dissolved in amorphous domains of PBSA matrix as inferred by DSC analysis.

Spherulitic morphology observed by POM

Spherulites of polymers can be packed in diversified patterns with influencing factors, resulting in various morphologies which can be visually observed by POM. Polarized optical images of PBSA and the complexes are presented in Fig. 11. It can be seen that spherulites of pristine PBSA are ringless and compact. The spherulitic sizes are roughly uniform. After incorporation of 10 wt% TDP, the morphology of spherulites turns into concentric ring-banded structure. The concentric ring-banded pattern becomes clearer and more regular when TDP content increases to 20 wt%, and the band spacing decreases distinctly. The concentric ring bands have been observed in many polymer spherulites, which are generally interpreted as lamellar twisting resulting from stress build up during crystallization.[32] Blending with amorphous component usually facilitates the formation of banded spherulites and often decreases band spacing,[33,34] which is in accordance with our observations because that TDP exists in amorphous state in the PBSA matrix. When TDP content reaches up 30 wt%, a unique ring-banded pattern with a band spacing in the inner region much wider than that in the outer region is obtained. As far as our knowledge, this is the first time that such intriguing structure is observed. Yet its mechanism research would be beyond the scope of this study. It is also notable that sizes of PBSA spherulites become less uniform with the addition of TDP, which agrees well with previous prediction by DSC analysis.

CONCLUSIONS

The intermolecular interactions, crystallization and melting behavior, crystal structure and morphology variations of PBSA/TDP complexes prepared by melt blending have been investigated in this work. FTIR analysis ascertains that intermolecular hydrogen bonding formed between carbonyl group of PBSA and hydroxyl group of TDP. Further quantitative analysis indicated that the fraction of hydrogen bonded carbonyl groups in PBSA increased with TDP content. The crystallization of PBSA was hindered by introduction of hydrogen bonding, which was indicated by decreased crystallization temperature, melting temperature, crystallinity and increased $t_{1/2}$ derived from Avrami equation. Avrami exponent n was calculated within the range of 2.4 to 2.8, which was ascribed to two to three-dimensional crystal growth with a combination of homogeneous and heterogeneous nucleation under investigated conditions. Analysis based on Lauritzen–Hoffman theory suggested that the fold surface energy (σ_e) and work of chain folding (q) increased with TDP incorporation in isothermal crystallization process. POM observation exhibited that morphology of PBSA crystallites changed distinctly from compact spherulites to

concentric ring-banded spherulites. Band spacing increased with TDP addition within the range of 0–20 wt%. We also observed a peculiar ring-banded pattern with discrepant band spacing for the first time in sample with 30 wt% TDP, whose formation mechanism remains to be discussed.

Acknowledgements

This work is financially supported by National Natural Science Foundation of China (No. 21264012).

REFERENCES

[1] L. Song and Z. Qiu, *Polymer Adv. Tech.*, *22*, 1642 (**2011**).
[2] J. Xu and B. Guo, *Biotechnol. J.*, *5*, 1149 (**2010**).
[3] P. Pan and Y. Inoue, *Prog. Polymer Sci.*, *34*, 605 (**2009**).
[4] D. Puppi, F. Chiellini, A. M. Piras and E. Chiellini, *Prog. Polymer Sci.*, *35*, 403 (**2010**).
[5] Z. Gan, H. Abe, H. Kurokawa and Y. Doi, *Biomacromolecules*, *2*, 605 (**2001**).
[6] Z. Gan, H. Abe and Y. Doi, *Macromol. Chem. Phys.*, *203*, 2369 (**2002**).
[7] M. Ren, J. Song, C. Song, H. Zhang, X. Sun, Q. Chen, H. Zhang and Z. Mo, *J. Polymer Sci. Polymer Phys.*, *43*, 3231 (**2005**).
[8] Z. Qi, H. Ye, J. Xu, J. Chen and B. Guo, *Colloid. Surf. A.*, *421*, 109 (**2013**).
[9] Y. He, B. Zhu, W. Kai and Y. Inoue, *Macromolecules*, *37*, 3337 (**2004**).
[10] S. Kuo, *J. Polymer Res.*, *15*, 459 (**2008**).
[11] Z. Qiu, *J. Appl. Polymer Sci.*, *104*, 3637 (**2007**).
[12] Z. Qiu and W. Yang, *J. Appl. Polymer Sci.*, *104*, 972 (**2007**).
[13] F. Yang, Z. Qiu and W. Yang, *Polymer*, *50*, 2328 (**2009**).
[14] M. Weng and Z. Qiu, *Thermochim. Acta.*, *575*, 262 (**2014**).
[15] S. W. Kuo, C. F. Huang and F. C. Chang, *J. Polymer Sci. Polymer Phys.*, *39*, 1348 (**2001**).
[16] T. Yu, Y. Zhou, Y. Zhao, K. Liu, E. Chen, D. Wang and F. Wang, *Macromolecules*, *41*, 3175 (**2008**).
[17] S. G. Lv, *Plastics Additives Handbook*, 1st ed.,, Light Industry Press, Beijing, **1988**.
[18] B. Fei, C. Chen, H. Wu, S. Peng, X. Wang, L. Dong and J. H. Xin, *Polymer*, *45*, 6275 (**2004**).
[19] F. Luo, F. Luo, Q. Xing, X. Zhang, H. Jiao, M. Yao, C. Luo and D. Wang, *Chin. J. Polymer Sci.*, *31*, 1685 (**2013**).
[20] Y. He, N. Asakawa and Y. Inoue, *J. Polymer Sci. Polymer Phys.*, *38*, 2891 (**2000**).
[21] J. Li, Y. He and Y. Inoue, *J. Polymer Sci. Polymer Phys.*, *39*, 2108 (**2001**).
[22] P. Si, F. Luo and M. Hai, *Chem. J. Chin. Univ.*, *36*, 188 (**2015**).
[23] H. Bai, Y. Zhang, Y. Zhang, X. Zhang and W. Zhou, *J. Appl. Polymer Sci.*, *101*, 1295 (**2006**).
[24] M. Avrami, *J. Chem. Phys.*, *8*, 212 (**1940**).
[25] C. Ge, P. Ding, L. Shi and J. Fu, *J. Polymer Sci. Polymer Phys.*, *47*, 655 (**2009**).
[26] R. Liao, B. Yang, W. Yu and C. Zhou, *J. Appl. Polymer Sci.*, *104*, 310 (**2007**).
[27] M. Yasuniwa, S. Tsubakihara, T. Satou and K. Iura, *J. Polymer Sci. Polymer Phys.*, *43*, 2039 (**2005**).
[28] J. D. Hoffman and J. J. Weeks, *J. Res. Natl. Bur. Stand. A*, *66*, 13 (**1962**).
[29] J. D. Hoffman and R. L. Miller, *Polymer*, *38*, 3151 (**1997**).
[30] S. Iannace and L. Nicolais, *J. Appl. Polymer Sci.*, *64*, 911 (**1997**).
[31] M. S. Nikolic and J. Djonlagic, *Polymer Degrad. Stabil.*, *74*, 263 (**2001**).
[32] B. Crist and J. M. Schultz, *Prog. Polymer Sci.*, (**2015**). DOI: 10.1016/j.progpolymsci.2015.11.006.
[33] Z. Qiu and W. Yang, *Polymer*, *47*, 6429 (**2006**).
[34] P. Xing, L. Dong, Y. An, Z. Feng, M. Avella and E. Martuscelli, *Macromolecules*, *30*, 2726 (**1997**).

[†]*Correction added on 20th of May, 2016, after first online publication: The Acknowledgement section has been added.*

